Received: 2 November 2023 | Revised: 30 January 2024 | Accepted: 13 March 2024

IET Control Theory & Applications

DOI: 10.1049/cth2.12645

The Institution of Engineering and Technology WILEY

ORIGINAL RESEARCH

Multiple adaptive factors based interacting multiple model estimator

Minxing Sun[1,2,3,4] | **Qianwen Duan**[1,2,3,5] | **Wanrun Xia**[1,2,3,4] | **Qiliang Bao**[1,2,3,5] | **Yao Mao**[1,2,3,5]

[1]National Key Laboratory of Optical Field Manipulation Science and Technology, Chinese Academy of Science, Chengdu, Sichuan, China

[2]Key Laboratory of Optical Engineering, Chinese Academy of Sciences, Chengdu, Sichuan, China

[3]Institute of Optics and Electronics, Chinese Academy of Sciences, Chengdu, Sichuan, China

[4]School of Electronic, Electrical and Communication Engineering, University of Chinese Academy of Sciences, Beijing, China

[5]School of Automation, Qingdao University, Qingdao, Shandong, China

Correspondence
Yao Mao, National Key Laboratory of Optical Field Manipulation Science and Technology, Chinese Academy of Science, Chengdu 610209, Sichuan, China.
Email: maoyao@ioe.ac.cn

Funding information
National Natural Science Foundation of China, Grant/Award Number: 62271109

Abstract

In the field of optoelectronic tracking, precisely modeling the motion equations of the tracked target is often challenging, and in some cases, they may even be entirely unknown. This necessitates the use of a robust state estimator for accurate state estimation. Additionally, atmospheric turbulence, variations in illumination, and intricate observation backgrounds may introduce a significant increase in observation noise for the tracked target. To address these challenges, one approach is to introduce adaptive factors, such as the Mahalanobis method, into the robust state estimator to enhance estimation accuracy. However, further exploration has revealed that adaptive factors designed using different methods offer unique advantages in scenarios with varying levels of noise amplification. In this paper, different adaptive factors are further combined using an interacting multiple model approach, allowing the designed state estimator to exhibit stronger adaptability to noise amplification. The stability and effectiveness of this algorithm are validated through program simulations, double reflection mirror experiment, and drone trace prediction, demonstrating its applicability and reliability in diverse scenarios.

1 | INTRODUCTION

In the fields of optoelectronic tracking [1, 2], free-space optical communication [3, 4], and trajectory prediction [5, 6], a significant challenge is the inability to obtain precise motion equations of the tracked targets. This issue is particularly pronounced when tracking non-cooperative, maneuvering targets, where we are limited to use generic models for estimation. There are inherent model errors between these generic state space models and the true state equations of the targets, necessitating the use of robust state estimators for the effective estimation and prediction tasks.

The concept of robust state estimation has been around for a long time, but its theory was formally introduced in the 1960s to address the instability issues in traditional optimization processes [7]. In the 1980s, Zames introduced the concept of H_∞ in control systems to reduce sensitivity to model uncertainties [8], which further led to the famous H_∞ estimation method and more related research [9-11]. Another important approach in robust state estimation is based on various improvements to the Kalman filter. Like the regularized robust state estimator was developed to modify parameters using an estimated parameter [12]. The interacting multiple model (IMM) state estimator [13], which utilizes the multiple motion models for estimation, can also be considered as a type of robust state estimator and has been widely applied in fields such as vehicle driving [14], manoeuvering target tracking [15], and event-based system [16].

Another challenge in the field of optoelectronic tracking is that observation errors, caused by variations in the optical path medium and limitations in sensor accuracy, are inevitable

[17, 18]. For instance, atmospheric turbulence leads to random fluctuations in the refractive index of the optical path medium, subsequently altering the intensity, coherence, and angle of light [19, 20]. This results in variations in brightness and positional jitter of the image captured by the camera. From the perspective of the estimator's state space model, these phenomena can be interpreted as an unpredictable increase in observation noise over certain periods.

One primary method to address the unpredictable increase in observation noise involves introducing adaptive factors. This entails assessing and adjusting the estimation error covariance, process noise covariance, and observation noise covariance based on residuals to enhance estimation accuracy [21-23]. The adaptive strong tracking cubature Kalman filter (ASTCKF) method proposed in [22] accomplishes corrections to all three, thereby enhancing estimator performance. However, it relies on an accurate motion model and does not meet the robustness requirements of optoelectronic tracking scenarios. A robust state estimator based on the Mahalanobis distance adaptive factor (MRE), proposed in [24], effectively addresses both model errors and spikes in observation noise, yet this adaptive factor is still not the optimal solution. Through a broader exploration of different adaptive factor design methods, we find that robust estimators (RMARE and HRE) designed using RMA methods [25] and Huber methods [26] have advantages under low noise amplification scenarios, while robust estimators (MRRE) designed using p-Huber (M-estimation) methods [27] excel in high noise amplification scenarios.

To realize robust state estimation in scenarios characterized by imprecise target motion models and intricate observation noise amplification, this study synthesizes five distinct sub-estimators. These include a fundamental robust estimator and four robust estimators, each augmented by adaptive factors derived from the Mahalanobis distance, Huber, p-Huber, or RMA methods. The unique strengths of these five estimators are synergistically combined through the application of the Interacting Multiple Model (IMM) method. This integration culminates in the development of the Multiple Adaptive Factors based Interacting Multiple Model Estimator (MAFIMME). This approach demonstrates enhanced adaptability to complex noise scenarios and notably improves estimation accuracy.

The Introduction now succinctly outlines the three principal contributions of this research: (1) Integration of Adaptive Factors: This work introduces a unique integration of three adaptive factors with robust state estimators, exploring their synergistic advantages for improved estimation. (2) Utilization of the IMM Method: It employs the IMM method to combine a conventional robust estimator with four distinct robust estimators, each enhanced by different adaptive factors. This strategy significantly boosts estimation accuracy in diverse noise environments.(3) Empirical Validation: The efficacy of the newly proposed algorithm is thoroughly validated through simulations, double reflection mirror experiments, and drone trace prediction, illustrating its practical utility and robustness.

The subsequent sections are organized as follows. Section 2 introduces the state space model and computational methods of the robust state estimator. Section 3 describes several design methods for adaptive factors. Section 4 explains how to use the IMM method to combine the estimation results of the different sub-estimators. Section 5 provides simulation and experiment results to demonstrate the effectiveness of the proposed MAFIMME algorithm. Finally, Section 6 presents the conclusion of this study.

2 | ROBUST STATE ESTIMATOR

In the field of optoelectronic tracking, the robust estimator's algorithm is formulated based on the motion model of the tracked target and structured in accordance with its associated cost function. This necessitates the introduction of (1) and (4) as foundational elements.

For the robust state estimator j, its establishment relies on the state space model of the tracked target given by (1):

$$\begin{aligned} x_j(k+1) &= (F_j(k) + \delta F_j(k))x_j(k) + (G_j(k) + \delta G_j(k))u_j(k), \\ y_j(k) &= H_j(k)x_j(k) + v_j(k). \end{aligned} \tag{1}$$

In this state equation, $x_j(k)$ and $y_j(k)$ represent the state and observed position values of the tracked target at k instance, respectively. The initial state $x_j(0)$, process noise $u_j(k)$, and observation noise $v_j(k)$ follow Gaussian distributions. $F_j(k)$, $G_j(k)$, and $H_j(k)$ are the pre-defined state transition matrix, process noise driving matrix, and state observation matrix, respectively. The errors between the actual motion model of the tracked target and the predefined state space equations are denoted by uncertainty quantities $\delta F_j(k)$ and $\delta G_j(k)$. The Kronecker symbol equation of δ_{ij} is defined as follows: when $i = j$, $\delta_{ij} = 1$; $\delta_{ij} = 0$, if $i \neq j$ satisfied. $u(k)$ and $v(k)$ satisfy (2) and (3):

$$\left[\delta F_j(k)\ \delta G_j(k)\right] = M_j \Delta_j [E_{f,j}(k)\ E_{g,j}(k)]; \tag{2}$$

$$\begin{aligned} &\mathrm{E}\left(\begin{bmatrix} x_j(0) \\ u_j(k) \\ v_j(k) \end{bmatrix}\begin{bmatrix} x_j(0) \\ u_j(k) \\ v_j(k) \end{bmatrix}^{\mathrm{T}}\right) \\ &= diag(\Pi_0, Q_j(k)\delta_{ij}, R_j(k)\delta_{ij}). \end{aligned} \tag{3}$$

Here, M_j is time-varying matrix, Δ_j is a scaling parameter that takes values from the range $[0, 1]$. $E_{f,j}(k)\ E_{g,j}(k)$ is the expectation of the model uncertainty. Π_0 is the state estimation covariance matrix. $Q_j(k)$ is the process noise covariance matrix. $R_j(k)$ is the observation noise covariance matrix. These parameters all require configuration based on the specific usage scenarios and application experience of the tracking system.

Based on the state space equation (4), the cost function can be constructed:

$$\begin{aligned}&\min_{\{x_j(k),u_j(k)\}}\max_{\{\delta F_j(k),\delta G_j(k)\}} E_1+E_2+E_3\\&E_1=\left\|x_j(k)-\hat{x}_j(k)\right\|^2_{\hat{P}_j^{-1}(k)}\\&E_2=\left\|u_j(k)\right\|^2_{Q_j^{-1}(k)}\\&E_3=\left\|y_j(k+1)-H_j(k+1)x_j(k+1)\right\|^2_{R_j^{-1}(k+1)}.\end{aligned}\tag{4}$$

Here, $\hat{x}_j(k)$ is the estimate of estimator j, $\hat{P}_j(k)$ is the estimation error covariance. The cost function could be reconstructed using following mathematical substitutions(5):

$$\begin{aligned}x&\leftarrow col\left\{x_j(k)-\hat{x}_j(k)\right\}\\b&\leftarrow y_j(k+1)-H_j(k+1)x_j(k+1)\\A&\leftarrow H_j(k+1)\left[F_j(k)\ G_j(k)\right]\\\delta A&\leftarrow H_j(k+1)M_j\Delta_j\left[E_{f,j}(k)\ E_{g,j}(k)\right]\\\delta b&\leftarrow -H_j(k+1)M_j\Delta_jE_{f,j}(k)\hat{x}_j(k)\\Q&\leftarrow\left(\hat{P}_j(k)^{-1}\oplus Q_j(k)^{-1}\right)\\W&\leftarrow R_j(k)^{-1}\\H&\leftarrow H_j(k+1)M_j\\E_a&\leftarrow\left[E_{f,j}(k)\ E_{g,j}(k)\right]\\E_b&\leftarrow -E_{f,j}(k)\hat{x}_j(k)\\\Delta&\leftarrow\Delta_i.\end{aligned}\tag{5}$$

By optimizing the convex optimization function, the optimal solution could be derived (6):

$$\hat{x}=\left[Q+A^TWA\right]^{-1}A^TWb.\tag{6}$$

Considering the uncertainties in the state space model, the adjusted optimal solution could be obtained as(7):

$$\hat{x}=\left[\hat{Q}+A^T\hat{W}A\right]^{-1}\left[A^T\hat{W}b+\hat{\lambda}E_a^TE_b\right],\tag{7}$$

where

$$\begin{aligned}\hat{Q}&=Q+\hat{\lambda}E_a^TE_a\\\hat{W}&=W+WH\left(\hat{\lambda}I-H^TWH\right)^+H^TW\\\hat{\lambda}&=\arg\min_{\lambda\geq\|H^TWH\|}G(\lambda)\\G(\lambda)&=\left\|x(\lambda)\right\|^2_{Q(\lambda)}+\lambda\left\|E_ax(\lambda)-E_b\right\|^2+\left\|Ax(\lambda)-b\right\|^2_{W(\lambda)}\\W(\lambda)&=W+WH\left(\lambda I-H^TWH\right)^+H^TW\\Q(\lambda)&=Q+\lambda E_a^TE_a\\x(\lambda)&=\left[Q(\lambda)+A^TW(\lambda)A\right]^{-1}\left[A^TW(\lambda)b+\lambda E_a^TE_b\right].\end{aligned}\tag{8}$$

A^+ means the pseudoinverse of the matrix A. Based on this optimal solution, we can derive the iterative formula for the robust state estimator j as follows (9)(10) [24]:

$$\begin{aligned}\hat{x}_j(k+1)&=\hat{F}_j(k)\hat{x}_j(k)+\hat{F}_j(k)P_j(k|k)H_j^T(k)\cdot\\&\quad\hat{R}_j^{-1}(k)(z(k)-H_j(k)\hat{x}_j(k))\\\hat{P}_j^{-1}(k+1)&=F_j(k)\hat{P}_j^{-1}(k)F_j^T(k)-\\&\quad\overline{K}_j(k)\overline{R}_{e,j}^{-1}(k)\overline{K}_j^T(k)+\hat{G}_j(k)\hat{Q}_j(k)\hat{G}_j^T(k)\\\overline{K}&=F_j(k)P_j(k)\overline{H}_j^T(k)\\\overline{R}_{e,j}(k)&=I+\overline{H}_j(k)P_j(k)\overline{H}_j^T(k)\\\overline{H}_j^T(k)&=\left[H_j^T(k)\hat{R}_j^{-T/2}(k)\sqrt{\hat{\lambda}_j(k)}E_{f,j}^T(k)\right].\end{aligned}\tag{9}$$

$$\begin{aligned}P_j(k|k)&=\left(\hat{P}_j^{-1}(k)+H_j^T(k)\hat{R}_j^{-1}(k)H_j^{-1}(k)\right)^{-1}\\&=\hat{P}_j(k)-\hat{P}_j(k)H_j^T(k)\left(\hat{R}_j(k)+\right.\\&\quad\left.H_j(k)\hat{P}_j(k)H_j^T(k)\right)^{-1}H_j(k)\hat{P}_j(k)\\\hat{Q}_j^{-1}(k)&=Q_j^{-1}(k)+\hat{\lambda}E_{f,j}^T\cdot\\&\quad\left[I+\hat{\lambda}E_{f,j}(k)P_j(k|k)\ E_{f,j}^T(k)\right]^{-1}E_{g,j}(k)\\\hat{R}_j(k+1)&=R_j(k+1)-\hat{\lambda}^{-1}\cdot\\&\quad H_j(k+1)M_jM_j^TH_j^T(k+1)\\\hat{G}_j(k)&=G_j(k)-\hat{\lambda}F_j(k)P_j(k|k)E_{f,j}^T(k)E_{g,j}(k)\\\hat{F}_j(k)&=\left(F_j(k)-\hat{\lambda}\hat{G}_j(k)\hat{Q}_j(k)E_{g,j}^T(k)E_{f,j}(k)\right)\cdot\\&\quad\left(I-\hat{\lambda}P_j(k|k)E_{f,j}^T(k)E_{f,j}(k)\right).\end{aligned}\tag{10}$$

3 | THE CONSTRUCTION OF THE ADAPTIVE FACTOR

In the actual operation of the photonic system, the state estimation algorithm may encounter scenarios where the observation noise increases unexpectedly, rendering the preset observation noise parameters ineffective. In this section, we will introduce several methods for constructing adaptive factors and incorporating them into the estimation algorithm to enable real-time assessment of the observation noise conditions and improve estimation accuracy. The adaptive factors discussed are all based on the deviation e_{k+1} between the observed value z_{k+1} and its estimated value $\hat{z}_{k+1}$. It is important to note that this deviation follows a Gaussian distribution. The differences in the design methods of various adaptive factors mainly lie in the handling of the deviation and the strategy for adjusting the observation noise covariance matrix.

3.1 | The Mahalanobis adaptive factor

The Mahalanobis adaptive factor requires initially calculating the Mahalanobis distance of the estimated bias using the following

equation, and the resulting value is denoted as the evaluation parameter γ_{k+1}:

$$\begin{aligned}\gamma_{k+1} &= {e_{k+1}}^T \cdot \left(\hat{R}_j(k+1) + H_j(k+1)P_{i+1}H_j^T(k+1)\right)^{-1} e_{k+1}\\ e_{k+1} &= z_{k+1} - \hat{z}_{k+1}\\ \hat{z}_{k+1} &= H_j(k+1)\hat{x}_j(k+1).\end{aligned} \tag{11}$$

Here, γ_{k+1} follows a chi-square distribution. Subsequently, the presence of observation noise amplification is assessed based on a predetermined confidence threshold χ_α^2. Assuming a confidence interval of $(1-a)$, corresponding to the threshold χ_α^2, if $\gamma_{k+1} > \chi_\alpha^2$, it can be inferred that the observation noise has experienced significant amplification, possibly due to atmospheric turbulence or other abnormal conditions. To ensure that the covariance of the estimation error e_{k+1} meets the confidence requirements, the evaluation parameter $\hat{R}_j(k+1)$ is adjusted using the following equation to obtain $\tilde{R}_j(k+1)$:

$$\begin{aligned}&\mathrm{P}(\gamma_{k+1} > \chi_\alpha^2) = \alpha\\ &\tilde{R}_j(k+1) = \frac{e_{k+1}^T e_{k+1}}{\chi_\alpha^2} - H_j(k+1)P_j(k+1)H_j^T(k+1).\end{aligned} \tag{12}$$

When $\gamma_{k+1} \le \chi_\alpha^2$, indicating that the difference e_{k+1} satisfies the confidence requirements. Let $\tilde{R}_j(k+1) = \hat{R}_j(k+1)$. Then it can be used in the iterative equations of the robust filter.

3.2 | The Huber adaptive factor

The Huber adaptive factor is designed based on Huber's M-estimation theory, utilizing the Huber compensation function to readjust the covariance matrix of observation noise. It also requires calculating the Mahalanobis distance of the estimated bias to obtain the evaluation parameter γ_{k+1}:

$$\begin{aligned}\gamma_{k+1} &= {e_{k+1}}^T \cdot \left(\hat{R}_j(k+1) + H_j(k+1)P_{i+1}H_j^T(k+1)\right)^{-1} e_{k+1}\\ e_{k+1} &= z_{k+1} - \hat{z}_{k+1}\\ \hat{z}_{k+1} &= H_j(k+1)\hat{x}_j(k+1).\end{aligned} \tag{13}$$

Similarly, the presence of observation noise amplification is determined by a predetermined confidence threshold χ_α^2. If $\gamma_{k+1} > \chi_\alpha^2$, it indicates the occurrence of exceptional circumstances requiring adjustment of the observation noise covariance parameter $\hat{R}_j(k+1)$. However, the adjustment strategy is modified as (14):

$$\begin{aligned}&\mathrm{P}(\gamma_{k+1} > \chi_\alpha^2) = \alpha\\ &\tilde{R}_j(k+1) = \frac{\hat{R}_j^{1/2}(k+1)\gamma_{k+1}\hat{R}_j^{1/2}(k+1)}{\chi_\alpha^2}.\end{aligned} \tag{14}$$

If no noise amplification is detected, let $\tilde{R}_j(k+1) = \hat{R}_j(k+1)$.

3.3 | The p-Huber adaptive factor

The p-Huber adaptive factor utilizes the same rules for detecting exceptional circumstances by calculating the evaluation parameter γ_{k+1} and determining whether to adjust $\hat{R}_j(k+1)$ based on the confidence threshold χ_α^2.

$$\begin{aligned}\gamma_{k+1} &= {e_{k+1}}^T \cdot \left(\hat{R}_j(k+1) + H_j(k+1)P_{i+1}H_j^T(k+1)\right)^{-1} e_{k+1},\\ e_{k+1} &= z_{k+1} - \hat{z}_{k+1},\\ \hat{z}_{k+1} &= H_j(k+1)\hat{x}_j(k+1).\end{aligned} \tag{15}$$

The adjustment strategy employs a piecewise equivalent weight function with the requirement of presetting two threshold points, $\chi_{\alpha1}^2$ and $\chi_{\alpha2}^2$, for determining the adjustment strategy. Specifically, a confidence interval of $(1-\alpha_1)$ corresponds to the threshold $\chi_{\alpha1}^2$, and $(1-\alpha_2)$ for $\chi_{\alpha2}^2$. When $\gamma_{k+1} > \chi_{\alpha1}^2$, denoted as $\mathrm{P}(\gamma_{k+1} > \chi_{\alpha1}^2) = \alpha_1$, it is considered that the observed value is erroneous and a non-acceptance decision is made, setting $\hat{R}_j(k+1) = \infty$. If $\chi_{\alpha1}^2 \ge \gamma_{k+1} > \chi_{\alpha2}^2$ is satisfied, which means $\mathrm{P}(\gamma_{k+1} > \chi_{\alpha2}^2) \approx \alpha_2$, it is considered that the observation noise amplification has occurred. The following adjustment (16) is performed on $\hat{R}_j(k+1)$ to readjust the covariance of e_{k+1} to meet the confidence requirements. $P(.)$ represents the probability of the event.

$$\tilde{R}_j(k+1) = \frac{\hat{R}_j(k+1)}{\left(\chi_{\alpha2}^2/\gamma_{k+1}\right)^{1/2}}. \tag{16}$$

If $\gamma_{k+1} \le \chi_{\alpha2}^2$, indicating that the difference e_{k+1} satisfies the confidence requirement, let $\tilde{R}_j(k+1) = \hat{R}_j(k+1)$. Then incorporate $\tilde{R}_j(k+1))$ into the iterative equation of the robust filter for further computation.

3.4 | The RMA adaptive factor

The design method for the evaluation parameter used in this adaptive factor is slightly different from those mentioned above. It is based on the principle of the smooth approximation function $f_u = \sqrt{x^2 + \mu^2}$ and utilizes the Mahalanobis distance as a foundation. A small real number is added to the Mahalanobis distance for correction, resulting in the evaluation parameter γ_{k+1} as follows (17):

$$\begin{aligned}\gamma_{k+1} &= 0.001 + e_{k+1}^T \cdot \left(\hat{R}_j(k+1) + H_j(k+1)P_{i+1}H_j^T(k+1)\right)^{-1} e_{k+1},\\ e_{k+1} &= z_{k+1} - \hat{z}_{k+1},\\ \hat{z}_{k+1} &= H_j(k+1)\hat{x}_j(k+1).\end{aligned} \tag{17}$$

Furthermore, the observed noise covariance $\hat{R}_j(k+1)$ is adjusted timely based on the preset confidence threshold χ_α^2. Specifically, a confidence interval of $1-a$ corresponds

ALGORITHM 1 The algorithm of robust estimator with adaptive factor.

1: Initialization: presuppose $\hat{x}_j(0)$, $P_j(0)$ and parameters for noise or uncertainties that mentioned in Section 2
2: **while** *using adaptive factor A's strategy*, **do**
3: *calculate* γ_{k+1}
4: **if** $\gamma_{k+1} > \chi^2_\alpha$ **then**
5: *adjust* $\hat{R}_j(k)$ *to* $\tilde{R}_j(k)$
6: **else**
7: *let* $\tilde{R}_j(k) = \hat{R}_j(k)$
8: **end if**
9: Substitute $\hat{R}_j(k)$ to $\tilde{R}_j(k)$ and execute (9) and (10) to obtain $\hat{x}_j(k+1)$ and $P_j(k+1)$
10: **end while**

to the threshold χ^2_α. If $\gamma_{k+1} > \chi^2_\alpha$, the following adjustment is performed on $\hat{R}_j(k+1)$ to readjust the covariance of e_{k+1} to meet the confidence requirements. Otherwise, $\tilde{R}_j(k+1) = \hat{R}_j(k+1)$.

$$\begin{aligned} &\mathrm{P}(\gamma_{k+1} > \chi^2_\alpha) = \alpha \\ &\tilde{R}_j(k+1) = \gamma_{k+1}\hat{R}_j(k+1). \end{aligned} \tag{18}$$

3.5 | Combining adaptive factors with robust state estimators

The integration of adaptive factors with robust state estimators is performed as follows. For the robust estimator j, after obtaining the observation value z_{k+1}, it is necessary to evaluate whether observation noise amplification has occurred. Which is based on the one-step predicted value of the estimated state $\hat{x}_j(k+1)$ and uses one of the adaptive factor calculation methods described above. If amplification is detected, the adjusted observation noise value $\tilde{R}_j(k+1)$ is obtained using the corresponding function, and the robust state estimation is performed by incorporating the adaptive factor. The specific algorithm flow is outlined as Algorithm 1.

4 | INTERACTING ROBUST STATE ESTIMATOR

The IMM state estimator is both an estimation and evaluation method. In brief, it involves multiple sub-estimators that simultaneously estimate the same observation value and produce different estimation results. The IMM approach, at a higher level, evaluates and assigns weights to the estimation results of each sub-estimator based on the observation value and historical data, ultimately outputting the final estimate. The MAFIMME method proposed in this paper leverages the IMM approach to integrate robust state estimators with different adaptive factors, resulting in improved estimation outcomes. The specific steps of the algorithm can be summarized as follows:

4.0.1 | Initialization

Construct the probability transition matrix P for each sub-robust state estimator, in which p_{ij} represents the probability of noise amplification transitioning from model i to model j.

$$P = \begin{bmatrix} p_{11} & \cdots & p_{1r} \\ \cdots & \cdots & \cdots \\ p_{r1} & \cdots & p_{rr} \end{bmatrix}. \tag{19}$$

The initial probabilities for each sub-estimator model μ_j are also need to be specified

4.0.2 | Input interaction

In this step, following parameters need to be computed for sub-robust state estimator j: the predicted probability $\bar{c}_j$, the mixed probability $\mu_{ij}(k-1)$ from sub-estimator i to sub-estimator j, the mixed state estimation value $\hat{X}_j(k-1)$, and the mixed covariance estimation value $P_j(k-1)$. The calculation methods for these values are as (20).

$$\begin{aligned} \bar{c}_j &= \sum_{i=1}^{r} p_{ij}\mu_i(k-1), \\ \mu_{ij}(k-1) &= \sum_{i=1}^{r} p_{ij}\mu_i(k-1)/\bar{c}_j, \\ \hat{X}_j(k-1) &= \sum_{i=1}^{r} \hat{x}_j(k)\mu_{ij}(k-1), \\ P_j(k-1) &= \sum_{i=1}^{r} \mu_{ij}(k-1)\{\hat{P}_j(k-1), \\ &\quad + [\hat{x}_j(k-1) - \hat{X}_j(k-1)] \cdot [\hat{x}_j(k-1) - \hat{X}_j(k-1)]^T\}. \end{aligned} \tag{20}$$

4.0.3 | Individual execution of sub-estimators

Each sub-robust state estimator independently utilizes a specific adaptive factor and performs estimation using the mixed state estimation value $\hat{X}_j(k-1)$ and corresponding covariance $P_j(k-1)$. Their outputs are the estimation value $\hat{x}_j(k)$ and estimation covariance $\hat{P}_j(k)$.

4.0.4 | Output interaction

The IMM algorithm evaluates the confidence of each sub-estimator based on their estimation results. The formulas for

confidence evaluation μ_j is calculated as (21).

$$\begin{aligned}
\mu_j(k) &= \Lambda_j(k)\bar{c}_j / c,\\
c &= \sum_{j=1}^{r} \Lambda_j(k)\bar{c}_j,\\
\Lambda_j(k) &= \frac{1}{(2\pi)^{n/2}\left|S_j(k)\right|^{1/2}} exp\left\{-\frac{v_j^T(k)S_i^{-1}(k)v_j(k)}{2}\right\},\\
v_j(k) &= z(k) - H_j(k)\hat{x}_j(k),\\
S_j(k) &= H_j(k)\hat{P}_j(k)H_j^T(k) + R_j(k).
\end{aligned} \tag{21}$$

4.0.5 | IMM estimation

In this step, the IMM algorithm combines the estimation results of each sub-robust state estimator by weighting them according to their confidence levels μ_j. This process yields the estimation output $\hat{x}(k)$ and covariance $\hat{P}(k|k)$ of the entire estimator.

$$\begin{aligned}
\hat{x}(k) &= \sum_{j=1}^{r} \hat{x}_j(k)\mu_j(k),\\
\hat{P}(k|k) &= \sum_{j=1}^{r} \mu_j(k)\{\hat{P}_j(k)\\
&\quad + [\hat{x}_j(k) - \hat{x}(k)] \cdot [\hat{x}_j(k) - \hat{x}(k)]^T\}.
\end{aligned} \tag{22}$$

5 | SIMULATION AND EXPERIMENT

5.1 | Simulation

To validate the effectiveness of the proposed method, this section conducts simulations on the following seven robust state estimators: (1) the proposed multiple adaptive factors based interacting multiple model estimator (MAFIMME), (2) the original robust state estimator (RE), (3) the robust estimators with MR adaptive factor (MRRE), (4) the robust estimators with Huber adaptive factor (HRE), (5) the robust estimators with RMA adaptive factor (RMARE), (6) the robust estimators with Mahalanobis adaptive factor (MRE) and (7) the adaptive strong tracking cubature Kalman filter (ASTCKF) [22]. The simulation details and parameter descriptions are provided as follows:

The parameters used in each robust estimator or interacting robust state estimator are the same and are as (23).

$$\begin{aligned}
&F = \begin{bmatrix} 0.9802 & 0.0196 \\ 0 & 0.9802 \end{bmatrix}, G = \begin{bmatrix} 1 & 0 \\ 0 & 1 \end{bmatrix},\\
&H = \begin{bmatrix} 1 & 1 \end{bmatrix}, M = \begin{bmatrix} 0.0198 \\ 0 \end{bmatrix},\\
&Q = 0.02 * \begin{bmatrix} 1.9608 & 0.0195 \\ 0.0195 & 1.9605 \end{bmatrix}, R_0 = 1,\\
&E_f = \begin{bmatrix} 0 & 5 \end{bmatrix}, E_g = \begin{bmatrix} 0 & 0 \end{bmatrix},\\
&x_0 = \begin{bmatrix} 0 \\ 0 \end{bmatrix}, P_0 = \begin{bmatrix} 1 & 0 \\ 0 & 1 \end{bmatrix}.
\end{aligned} \tag{23}$$

The specific parameters used in the interacting robust state estimator based on multiple adaptive factors are as (24):

$$\begin{aligned}
P &= \begin{bmatrix} 0.9 & 0.025 & 0.025 & 0.025 & 0.025 \\ 0.025 & 0.9 & 0.025 & 0.025 & 0.025 \\ 0.025 & 0.025 & 0.9 & 0.025 & 0.025 \\ 0.025 & 0.025 & 0.025 & 0.9 & 0.025 \\ 0.025 & 0.025 & 0.025 & 0.025 & 0.9 \end{bmatrix},\\
\mu_j &= \begin{bmatrix} 0.2 & 0.2 & 0.2 & 0.2 & 0.2 \end{bmatrix}.
\end{aligned} \tag{24}$$

Thresholds for the MR adaptive factor are $\chi^2_{\alpha 1} = 5.02$, $\chi^2_{\alpha 2} = 6.63$.

Threshold for the Huber adaptive factor is $\chi^2_{\alpha} = 6.63$.

Threshold for the RMA adaptive factor is $\chi^2_{\alpha} = 6.63$.

Threshold for the Mahalanobis adaptive factor is $\chi^2_{\alpha} = 6.63$.

The chi-square test threshold of 5.02 corresponds to the 97.5% distribution expectation for a one-dimensional random variable, while the chi-square test threshold of 6.63 corresponds to the 99% distribution expectation for a one-dimensional random variable in a statistical context.

In the process of simulating the motion of the tracked target and observation, the state transition equation used is

$$\begin{aligned}
x_i &= (F + M\Delta_i E_f)x_{i-1} + u_i\\
y_i &= Hx_i + v_i.
\end{aligned} \tag{25}$$

To simulate the occurrence of observation noise amplification, R_i, the covariance matrix of the observation noise u_i, is not a constant value. Instead, it is randomly generated from the range of $R_0 \sim aR_0$. Different values of parameter a represent different levels of observation noise amplification, that is selected from 1, 5, 10, 20, 30, 50, 75, 100.

Next, following the robust state estimator design method described earlier, we used C programming to generate trajectories and obtain observations for each level of observation noise amplification (i.e. different parameter values of a).For each condition, a comprehensive series of 500 trajectory generations and observation collections were conducted, with each trajectory comprising 100 observation points. The accumulated root mean square estimation error ($AErr_{E,a}$) for seven estimators and the reduction ratio of accumulated estimation error ($Ratio_{E,a}$) for six state estimators were then calculated.

$$AErr_{E,a} = \sum_{I=1}^{500}\sum_{J=1}^{100}\sqrt{\frac{1}{2}\sum_{K=1}^{2}\left(X_{a,I,J,K} - \hat{X}_{E,a,I,J,K}\right)^2}, \tag{26}$$

$$Ratio_{E,a} = \frac{AErr_{RE,a} - AErr_{E,a}}{AErr_{RE,a}}, \tag{27}$$

where $X_{a,I,J,K}$ represents the true value of the K dimension state at the J point of the I simulation trajectory when the maximum noise amplitude is $aR0$; $\hat{X}_{E,a,I,J,K}$ represents the estimated value of Estimator E at (a, I, J, K); $AErr_{E,a}$ refers to the accumulated estimation error of the estimator E; $AErr_{RE,a}$ refers to the accumulated estimation error of the estimator RE.

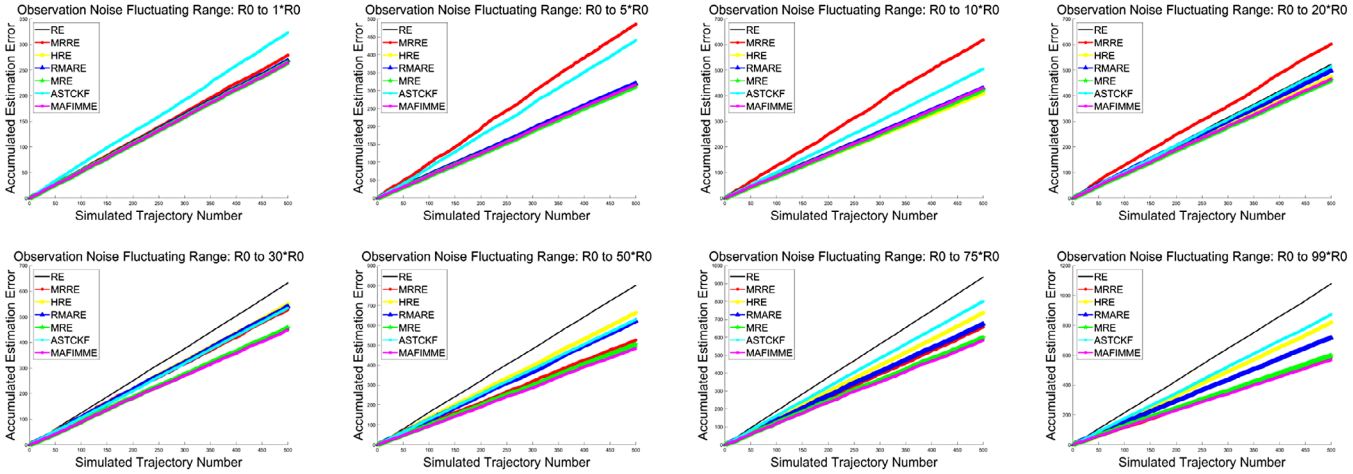

FIGURE 1 Accumulated estimation error under different observation noise amplification conditions.

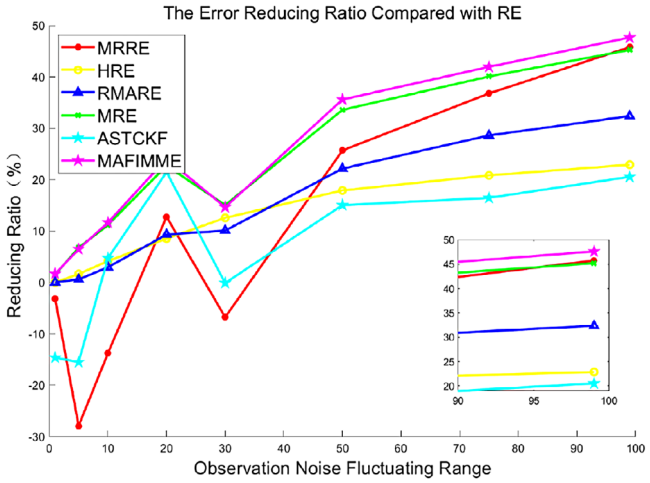

FIGURE 2 Comparison of the reduction ratio of estimation error between MAFIMME and other robust estimators.

According to Figure 1, the simulation results reveal that each of the six estimators, apart from MAFIMME, demonstrates unique advantages at varying levels of observation noise amplification, with each achieving the lowest accumulative estimation error in certain specific scenarios. Notably, the magenta curve, representing MAFIMME's accumulated estimation error across different noise amplification levels, consistently maintains the highest level of estimation accuracy.

In Figure 2, using the accumulative estimation error of the traditional robust filter as the baseline, a comparison is made among MAFIMME, MRRE, HRE, RMARE, MRE, ASTCKF in terms of the reduction ratio of accumulative estimation error. This figure quantitatively reflects the capability of MAFIMME to compensate noise amplification and its relative advantage over single adaptive factor-based robust state estimators. Furthermore, as detailed in Table 1, the reduction ratio of accumulated estimation error unequivocally highlights MAFIMME's excellent universality and its near-optimal estimation capabilities, underscoring its ability to effectively integrate the advantages of various adaptive factors.

TABLE 1 The reduction ratio of accumulated error compared with traditional robust estimator in different levels of noise amplification.

Maximum Noise	1R0	5R0	10R0	20R0	30R0	50R0	75R0	99R0
MRRE	−3.21	−27.92	−13.77	12.75	−6.77	25.67	36.75	45.76
HRE	0.00	1.64	4.15	8.52	12.55	17.89	20.81	22.90
RMARE	−0.00	0.58	2.95	9.30	10.08	22.14	28.58	32.35
MRE	1.54	6.71	11.18	22.68	15.03	33.55	40.07	45.21
ASTCKF	−14.62	−15.49	4.73	21.44	−0.11	15.03	16.45	20.54
MAFIMME	1.68	6.46	11.65	24.05	14.63	35.56	41.93	47.63

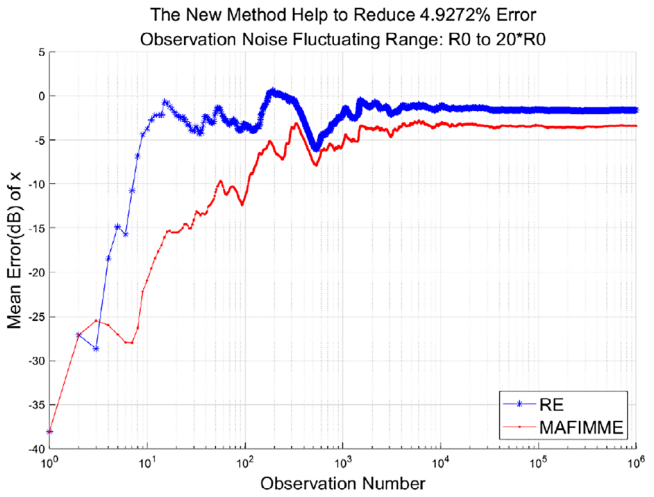

FIGURE 3 Comparison of the performance of MAFIMME with original RE.

In Figure 3, using a logarithmic coordinate system, a 1,000,000 steps simulation comparison is further demonstrated between MAFIMME and the original RE, validating the stability and effectiveness of the proposed method.

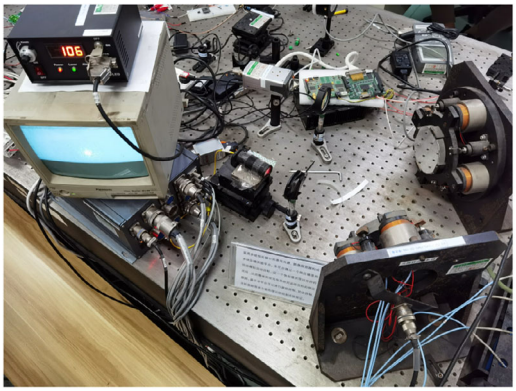

FIGURE 4 The double reflection mirrors experimental platform.

FIGURE 5 The control mirror.

5.2 | Experiment

The efficacy of the algorithm previously introduced was firstly validated on a double reflection mirrors experimental platform (Figure 4). This platform primarily comprises a laser generator, two fast steering mirrors with independent control boards, and a CCD camera. One of the fast steering mirrors is employed to simulate the motion of the tracked target, referred to as the disturbance mirror, while the other fast steering mirror is used to validate the control algorithm or state estimation algorithm, referred to as the control mirror (Figure 5). The operational procedure of this experimental platform is as follows: when the disturbance mirror moves independently, the spots of light within the camera's field of view move in synchrony. The control mirror, based on the offset of the light spot observed by the camera, is tasked to compensate the motion of the disturbance mirror, and maintain the light spot at the center of the field of view. Given that the camera sensor within this system introduces a delay of 0.06 s, with a data output frequency of 50 Hz, resulting in a data delay of 3 frames, a three steps estimator was employed to enhance the control performance of the system.

During the experimental process, the disturbance mirror performs sinusoidal motion with different amplitudes and frequencies on its X and Y axes. The control mirror, based on its own mirror tilt angles and the offset of the light spot observed by the camera, computed the target's position and made predictions accordingly. The experiment compared the prediction

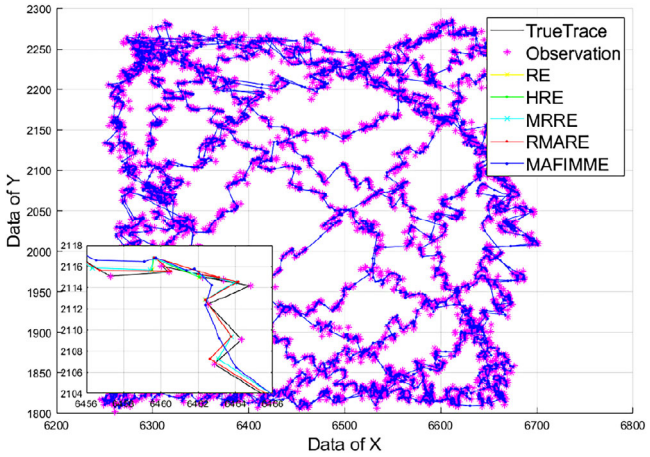

FIGURE 6 Spot trajectory and estimation results.

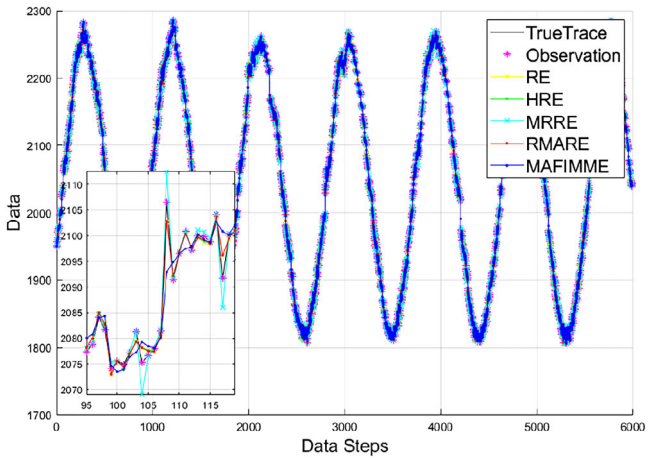

FIGURE 7 X-axis spot trajectory and estimation results.

results of five state estimation algorithms: MAFIMME (IMM Adaptive Robust Estimator), RE (Robust Estimator), RMARE (Adaptive Robust Estimator 1), HRE (Adaptive Robust Estimator 2), and MRRE (Adaptive Robust Estimator 3). The pixel position trajectory of the light spot within the camera's field of view and the corresponding prediction results are demonstrated in Figure 6.

When analyzing the data exclusively along the X-axis, as can be observed in Figure 7, it becomes evident that all the considered algorithms effectively realize noise suppression and position prediction.

By further plotting the estimation errors of various state estimation algorithms in Figure 8 and the accumulative estimation errors in Figure 9, it becomes evident that MAFIMME outperforms RE, MRRE, HRE, and RMARE by exhibiting smaller estimation biases, resulting in prediction results that closely approximate the actual light spot positions. Through calculations, it can be found that MAFIMME reduces the cumulative estimation errors by 3.6%, 3.6%, 26.8%, and 30.2% compared to RE, RMARE, HRE, and MRRE, respectively. This substantiates the engineering applicability and prediction precision advantages of MAFIMME.

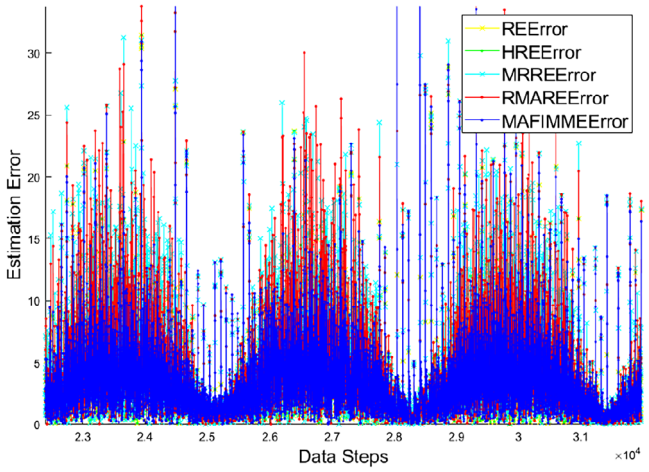

FIGURE 8 Estimation error.

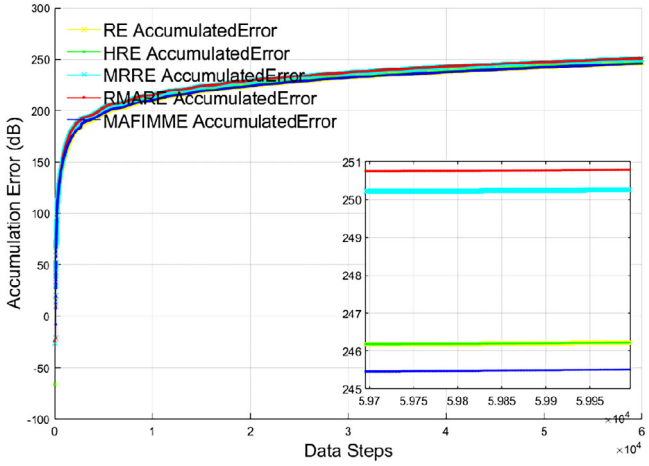

FIGURE 9 Accumulated estimation error.

FIGURE 10 The unmanned aerial vehicle.

The effectiveness of this algorithm was further validated in unmanned aerial vehicle (UAV) trajectory prediction. In this study, consumer-grade UAV product, specifically the DJI Mini 3 Pro (Figure 10), was employed for real flight experiments and GPS trajectory recording.

Based on the positions of the imaging equipment, optical axis direction, and field of view, the UAV's three-dimensional

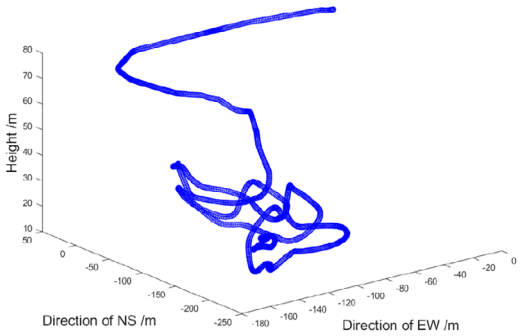

FIGURE 11 UAV's three-dimensional GPS trajectory.

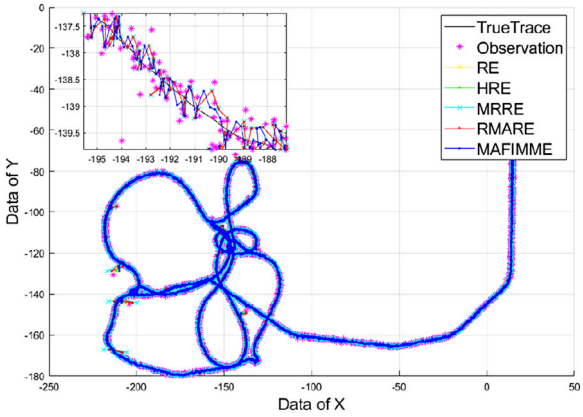

FIGURE 12 UAV's two-dimensional pixel trajectory.

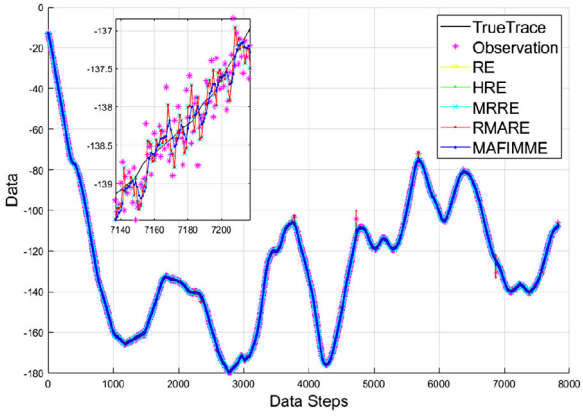

FIGURE 13 X-axis UAV trajectory.

GPS trajectory (Figure 11) was mapped to two-dimensional pixel locations within the camera frame. Subsequently, the MAFIMME, RE, RMARE, HRE, and MRRE algorithms were used to predict the target positions with artificially introduced three-step signal delays. These predictions were then compared with the actual position values (Figure 12).

Similarly, in this experiment, the X-axis data for both target trajectory and state estimation values were extracted and plotted (Figure 13). It is evident that the proposed MAFIMME

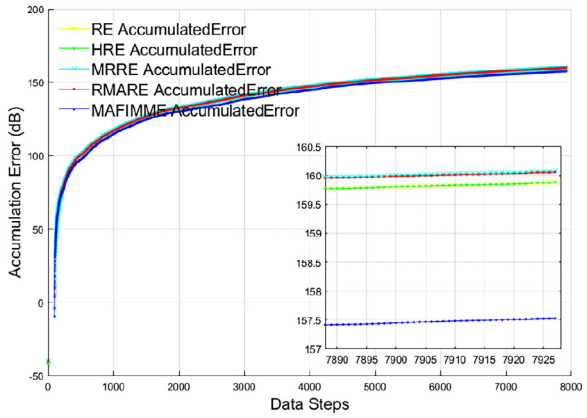

FIGURE 14 Accumulated estimation error.

algorithm continues to function effectively in real-world motion scenarios and achieves accurate predictions.

In this experiment, the accumulation estimation errors for different estimators were also computed (Figure 14). It is observable that, in comparison to the RE, RMARE, HRE, and MRRE methods, MAFIMME reduces the accumulation errors by 12.11%, 12.11%, 13.20%, and 13.09%, respectively. This demonstrates the applicability of the method in the field of real optoelectronic tracking and position estimation.

6 | CONCLUSION

In order to address the problem of complex observation noise amplification caused by factors, this study explored various methods for constructing adaptive factors. Then used adaptive factors to evaluate the scenarios of observation noise amplification and adjust the parameters of the estimation algorithm. However, different adaptive factors have unique advantages under different scenarios of observation noise amplification. It is not possible to identify a single best adaptive factor. Therefore, this study further employed the interacting multimodel approach to integrate the advantages of different adaptive factors, aiming to improve the estimation accuracy under complex observation noise amplification scenarios. The simulation and experiment results demonstrate that the proposed method possesses a universally applicable and stable suboptimal estimation capability, and its overall estimation performance surpasses any individual original method.

It should be noted that, despite offering improved estimation accuracy, MAFIMME also results in approximately 10 times the computational complexity of a single estimator. Such computational speed may be acceptable in lower-frequency optoelectronic tracking systems but could pose a significant burden for embedded or high-speed systems.

About future research, MAFIMME is proposed for linear estimation and Gaussian noise. Thus, relative estimation methods and adaptive factors for nonlinear and non-Gaussian noise scenarios are worth for further research. The interacting method in MAFIMME is also worth exploreing, its integrating ability could be further improved through modern method.

AUTHOR CONTRIBUTIONS

Minxing Sun: Conceptualization; data curation; formal analysis; funding acquisition; investigation; methodology; project administration; resources; software; validation; visualization; writing—original draft; writing—review and editing. **Qianwen Duan**: Conceptualization; formal analysis; investigation; methodology; writing—review and editing. **Wanrun Xia**: Conceptualization; data curation; project administration; validation. **Qiliang Bao**: Conceptualization; investigation; methodology; project administration; resources; supervision; writing—review and editing. **Yao Mao**: Investigation; methodology; project administration; resources; supervision; writing—review and editing.

CONFLICT OF INTEREST STATEMENT

The authors declare no conflicts of interest.

DATA AVAILABILITY STATEMENT

Data available on request from the authors.

ORCID

Yao Mao https://orcid.org/0000-0003-1785-2018

REFERENCES

1. Zhao, T., Tong, W., Mao, Y.: Hybrid nonsingleton fuzzy strong tracking Kalman filtering for high precision photoelectric tracking system. IEEE Trans. Ind. Inf. 19(3), 2395–2408 (2023)
2. Zhou, X., Mao, Y., Zhang, H., Nie, K.: Resonance compensation research of tip-tilt mirror's 2-DOF tracking-disturbance rejection problem. Sens. Actuators, A 346, 113837 (2022)
3. Wang, J.Y., Wang, J.B., Chen, M., Song, X.: Performance analysis for free-space optical communications using parallel all-optical relays over composite channels. IET Commun. 8(9), 1437–1446 (2014)
4. Deng, J., Xue, W., Liang, W., Zhou, X., Mao, Y.: On adjustable and lossless suppression to disturbances and uncertainties for nonminimum-phase laser pointing system. ISA Trans. 136, 727–741 (2023)
5. Lee, S.W., Kang, J., Shin, J., Paik, J.: Hierarchical active shape model with motion prediction for real-time tracking of non-rigid objects. IET Comput. Vision 1(1), 17–24 (2007)
6. Nejad, A.M., Shobeiri, S.M.: Three-dimensional route prediction algorithm based on minimal available information in wireless ad hoc sensor networks. In: IET Conference on Wireless Sensor Systems (WSS 2012), pp. 1-5. IEEE, Piscataway (2012)
7. Huber, P.J.: Robust estimation of a location parameter. In: Kotz, S., Johnson, N.L. (Eds.) Breakthroughs in Statistics, pp. 492–518. Springer, New York (1992)
8. Zames, G.: Feedback and optimal sensitivity: Model reference transformations, multiplicative seminorms, and approximate inverses. IEEE Trans. Autom. Control 26(2), 301–320 (1981)
9. Khargonekar, P.P., Rotea, M.A.: Mixed H/sub 2//H/sub infinity / control: A convex optimization approach. IEEE Trans. Autom. Control 36(7), 824–837 (1991)
10. Simon, D.: Optimal State Estimation: Kalman, H Infinity, and Nonlinear Approaches. John Wiley & Sons, Hoboken, NJ (2006)
11. Li, W., Zhu, Z., Zhou, G., Chen, G.: Optimal H_i/H_∞ fault-detection filter design for uncertain linear time-invariant systems: An iterative linear matrix inequality approach. IET Control Theory Appl. 7(8), 1160–1167 (2013)
12. Sayed, A.H.: A framework for state-space estimation with uncertain models. IEEE Trans. Autom. Control 46(7), 998–1013 (2001)
13. Blom, H., Barshalom, Y.: The interacting multiple model algorithm for systems with Markovian switching coefficients. IEEE Trans. Autom. Control 33(8), 780–783 (1988)

14. Zhang, L., Mao, X.: Vehicle density estimation of freeway traffic with unknown boundary demand-supply: An interacting multiple model approach. IET Control Theory Appl. 9(13), 1989–1995 (2015)
15. Fu, X., Shang, Y., Yuan, H.: Improved diagonal interacting multiple model algorithm for manoeuvering target tracking based on H ∞ filter. IET Control Theory Appl. 9(12), 1887–1892 (2015)
16. Lee, S., Hwang, I.: Event-based state estimation for stochastic hybrid systems. IET Control Theory Appl. 9(13), 1973–1981 (2015)
17. Li, Y., Kang, D., Liu, B., Zhou, R., Shao, S., Li, X., et al.: Characteristic analysis of atmospheric turbulence from inland to ocean. In: 15th International Conference on Optical Communications and Networks (ICOCN), pp. 1–3. IEEE, Piscataway (2016)
18. Bolbasova, L., Gritsuta, A., Lavrinov, V., Lukin, V., Selin, A., Soin, E.: Measurements of atmospheric turbulence from image motion of laser beam by Shack-Hartmann wavefront sensor. In: 2019 Russian Open Conference on Radio Wave Propagation (RWP), Kazan, Russia, 2019, vol. 1, pp. 217–220. IEEE, Piscataway (2019)
19. Zhu, X., Kahn, J.M.: Free-space optical communication through atmospheric turbulence channels. IEEE Trans. Commun. 50(8), 1293–1300 (2002)
20. Chen, J., Guo, H., Liu, P., Wang, Y.: The summary on atmospheric disturbance problems in the motion imaging of high resolution earth observation system. In: Proceedings of 2011 International Conference on Electronic & Mechanical Engineering and Information Technology, vol. 8, pp. 3999–4003. IEEE, Piscataway (2011)
21. Zhang, H., Xie, J., Ge, J., Lu, W., Liu, B.: Strong tracking SCKF based on adaptive CS model for manoeuvring aircraft tracking. IET Radar Sonar Navig. 12(7), 742–749 (2018)
22. Ma, J., Guo, X.: Combination of IMM algorithm and ASTRWCKF for maneuvering target tracking. IEEE Access 8, 143095–143103 (2020)
23. Tang, Z., Liu, Y., Liu, T., Xu, X., Liu, J.: Adaptive weighted ridge regression estimator for time-varying sensitivity identification. IEEE Trans. Power Syst. 39(1), 2377–2380 (2024)
24. Sun, M., Mao, Y., Liu, H.: A robust state estimator with adaptive factor. IEEE Access 8, 144514–144521 (2020)
25. Peng, M.k., Guo, Y.h., Wang, J.d., Mou, J.m., Hu, Y.: Adaptive target tracking algorithm based on robust cubature Kalman filter. Control Theory Appl. 37(4) (2020)
26. Jiang, H., Cai, Y.l.: Robust Gaussian-sum ensemble Kalman filter and its application in bearings-only tracking. Control Theory Appl. 35(2), 70116 (2018)
27. Wu, H., Chen, S.X., Yang, B.F., Chen, K.: Robust cubature Kalman filter target tracking algorithm based on generalized M-estiamtion. Acta Phys. Sin. 64(21), 218401 (2015)

How to cite this article: Sun, M., Duan, Q., Xia, W., Bao, Q., Mao, Y.: Multiple adaptive factors based interacting multiple model estimator. IET Control Theory Appl. 18, 1059–1069 (2024). https://doi.org/10.1049/cth2.12645